NANO LETTERS

2008
Vol. 8, No. 2
473−477

SP1 Protein-Based Nanostructures and Arrays

Izhar Medalsy,[†,£] Or Dgany,[‡,£] Mukhles Sowwan,[†,§] Hezy Cohen,[†] Alevtyna Yukashevska,[||] Sharon G. Wolf,[⊥] Amnon Wolf,[#] Abraham Koster,[+] Orna Almog,[¶] Ira Marton,[#] Yehonathan Pouny,[#] Arie Altman,[‡] Oded Shoseyov,[*,‡] and Danny Porath[*,†]

Physical Chemistry Department and Center for Nanoscience and Nanotechnology, The Hebrew University, Jerusalem 91904, Israel, The Robert H. Smith Institute of Plant Sciences and Genetics in Agriculture, The Faculty of Agriculture, The Hebrew University, Rehovot 76100, Israel, Materials Engineering Department, Al Quds University, East Jerusalem, Israel, Utrecht University, 3584 CH Utrecht, the Netherlands, Electron Microscopy Unit, Weizmann Institute of Science, Rehovot 76100 Israel, Fulcrum SP Ltd. P.O. Box 3206, Herzliya 46104, Israel, Department Molecular Cell Biology, Leiden University Medical Center, Leiden 2300 RC, The Netherlands, and Department of Clinical Biochemistry, Health Sciences Faculty, Ben-Gurion University, Beer-Sheva 84105, Israel

Received September 24, 2007; Revised Manuscript Received December 4, 2007

ABSTRACT

Controlled formation of complex nanostructures is one of the main goals of nanoscience and nanotechnology. Stable Protein 1 (SP1) is a boiling-stable ring protein complex, 11 nm in diameter, which self-assembles from 12 identical monomers. SP1 can be utilized to form large ordered arrays; it can be easily modified by genetic engineering to produce various mutants; it is also capable of binding gold nanoparticles (GNPs) and thus forming protein–GNP chains made of alternating SP1s and GNPs. We report the formation and the protocols leading to the formation of those nanostructures and their characterization by transmission electron microscopy, atomic force microscopy, and electrostatic force microscopy. Further control over the GNP interdistances within the protein–GNP chains may lead to the formation of nanowires and structures that may be useful for nanoelectronics.

One of the main challenges of the research within the realm of nanoscience and nanotechnology is the ability to form complex combinations of nanomaterials and organize them in a controlled way on surfaces or in wire forms.[1−7] Examples of organized structures can be two-dimensional (2D) protein arrays that were presented by Trent and by Guckenberger,[5,8,9] ordered arrays of nanosized elements templated by DNA,[10−16] hybrids of nanoparticles and bio-molecules,[17−20] nanowires displaying nonlinear electric behavior,[21] and biosensors.[22−25] Such structures can be useful for applications ranging from nanoelectronics to medicine.

Throughout the years different strategies have been developed to form nanostructures in a controlled way. One possibility is through lithography. This method is, however, difficult to implement for complex structures on the nanometer scale, especially for large and dense configurations. A popular alternative is through self-assembly of suitable building blocks that enable structuring and well-defined formation. Ordering such building blocks, for example, quantum dots in arrays or in close proximity, may enable us to utilize the full electronic potential of those particles regarding data storage and current transport (nonlinear as well). To serve as such building blocks, the candidates for template structures must be stable, well-defined, well-controlled, and should possess capability for structural hierarchy. A suitable building block that can be utilized for such patterning scaffolds may be very useful for the evolving field of nanoscience.

Proteins are attractive candidates for this task due to their well-defined structure and the feasibility of structural modifications by genetic engineering. Such manipulations enable optimization of the self-assembly and the ability to attach various inorganic nanoparticles through proteinaceous affinity tags. One of the drawbacks of proteins in general is, however,

* Corresponding authors. E-mail: (D.P.) porath@chem.ch.huji.ac.il; (O.S.) shoseyov@agri.huji.ac.il.
† The Hebrew University, Jerusalem.
‡ The Hebrew University, Rehovot.
§ Al Quds University.
|| Utrecht University.
⊥ Weizmann Institute of Science.
Fulcrum SP Ltd.
+ Leiden University Medical Center.
¶ Ben-Gurion University.
£ These authors contributed equally to this paper.

10.1021/nl072455t CCC: $40.75
Published on Web 01/15/2008

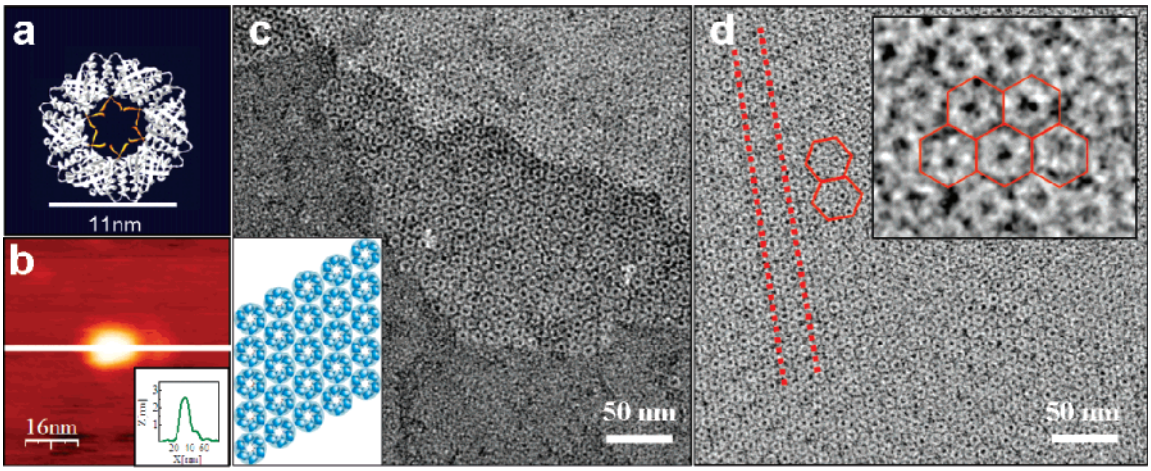

Figure 1. Wild type SP1 protein structure and two-dimensional arrays. (a) X-ray structure of the W.T. SP1, showing the N-termini of the monomers in orange. (b) High-resolution AFM image (tip apex ~1 nm) of a single dodecamer and its cross section (inset). (c) TEM image of ordered W.T. SP1 arrays (one and two monolayers). Inset: schematic representation of a W.T. SP1 array. (d) TEM imaging of a part of a highly ordered and continuous array of W.T. SP1. The red lines and 2 adjacent hexagons in the continuous array, emphasize the diagonal and hexagonal ordering patterns of the W.T. SP1 arrays. The inset shows an enlargement of a discrete region with superimposed hexagons (each hexagon is superimposed on a W.T. SP1 dodecamer). Staining was performed using uranyl acetate.

their sensitivity to different environmental conditions such as temperature, pH, proteases, etc. A protein that is both durable and can direct different functional groups is of great interest.

We have previously reported the formation of enzyme protein chains, using Stable Protein 1 (SP1) as a molecular scaffold for glucose oxidase.[22] In the present letter, we report large ordered, microns in size, arrays of wild type (W.T.) SP1 and two new variants of the SP1 protein that interact with gold nanoparticles (GNPs) through histidine[26] Ni-NTA chemistry. These two new variants (6His-SP1 and 6HΔSP1) form single SP1−GNP units and alternating protein−GNP chain structures

SP1 is a homo-oligomeric protein, isolated from aspen (*Populus tremula*) plants.[27,28] The protein complex is a 148.8 kDa homododecamer (12-mer). Its crystal structure, shown in Figure 1a, reveals a ring, 11 nm in diameter, with an inner pore of 2−3 nm and width of 4−5 nm.[29] The N terminal region of the SP1 dodecamer faces the inner pore of the ring (N-termini in orange in Figure 1a) and is tolerant to amino acid deletions and additions.[26] The three-dimensional morphology of a single SP1 protein complex on freshly cleaved mica was measured using high-resolution tip (tip apex ~1 nm) in dynamic mode atomic force microscopy (AFM) (Nanotec Electronica, Madrid),[30] as shown in Figure 1b. The measured height and width can be seen in the cross section in the inset. The measured diameter is 13 ± 1 nm, slightly larger than the SP1 diameter, 11 nm, due to tip convolution, and the height, ~2.5 nm, is lower than the value obtained from the crystal structure, 4−5 nm, due to the surface attraction.

One of the important potential applications of a protein scaffold is to impose lateral organization of ultradense docking sites on a surface. Such docking arrays can be used to anchor quantum dots for memory applications and to anchor other enzymes to speed up recognition events for biosensors and other applications. The formation of such an array was reported by Trent et al.[5] for chaperonins, using site-directed mutagenesis. Using the W.T. SP1 ring proteins, we formed large ordered arrays with a periodicity of ~11 nm. The array was assembled in the following way: a mixture of phospholipids (1,2-dioleoyl-3-trimethylammonium-propane/ 1,2-dioleoyl-*sn*-glycero-3-phosphocholine, Sigma-Aldrich Co.) was spread on 30 μL of protein solution and allowed to incubate for 20 min in Teflon wells. A transmission electron microscopy (TEM) carbon-evaporated grid was laid on the drop for 1 min, withdrawn, dried, and stained with uranyl acetate. This method has been commonly used to acquire 2D arrays for a variety of soluble and nonsoluble proteins.[31] TEM imaging revealed a well-defined hexagonal closed pack arrangement of the SP1 proteins with regular periodicity over microns. The clear close-packed organization of the arrays is shown in the TEM images shown in Figure 1c,d and in the enlargement in the inset of Figure 1d. Note the ordered layers in Figure 1c and the hexagonal long range arrangement in both examples. In the inset of Figure 1c, we show a scheme of the array organization.

A six histidine tag was incorporated to the N termini of the SP1 (creating the variant 6His-SP1) to enable binding of Ni-NTA conjugates. This variant was expressed in *E. coli* and purified from the bacterial lysate by Ni-NTA agarose beads (P-6611, Sigma Chemicals, St. Louis, MO) according to the supplier's protocol (www.sigmaaldrich.com/sigma/bulletin/p6611bul.pdf) except that the elution buffer contained 400 mM imidazole.

The extreme stability of the 6His-SP1 protein to detergents and high temperature is demonstrated in Figure 2. The stability of the protein to detergents and heat treatment is shown by sodium dodecyl sulfate polyacrylamide gel electrophoresis (SDS-PAGE) analysis in Figure 2a, where the 6His-SP1 complex is not dissociated in the presence of SDS as demonstrated in lane 3 (the protein dissociates only when preboiled in sample application buffer as in lane 4) and does not precipitate upon heating (lanes 3 and 4) in contrast to

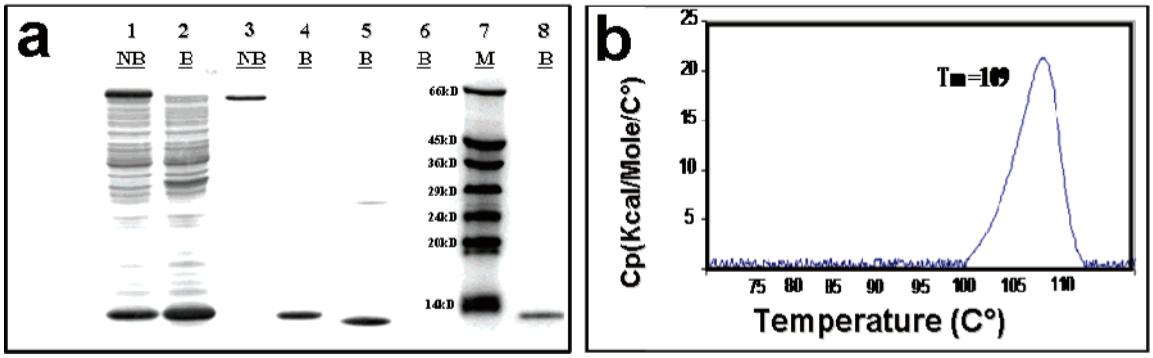

Figure 2. Biochemical analysis of the 6His-SP1 mutant. (a) SDS-PAGE analysis of 6His-SP1. Lanes 1 and 2, 6His-SP1 bacterial extract after lysis; lanes 3 and 4, 6His-SP1 bacterial extract after lysis + heat treatment; lane 5, W.T protein; lane 6, W.T. elution after binding to Ni-NTA agarose; lane 7, molecular weight marker; lane 8, 6His-SP1 elution after binding to Ni-NTA agarose. (NB) - Not boiled with sample application buffer (SAB) before loading; (B) - boiled with SAB before loading. SP1 and 6His-SP1 are dissociated to monomers when preboiled with SAB before loading on gel. (b) DSC curve of 6His-SP1 showing a melting temperature of 109 °C.

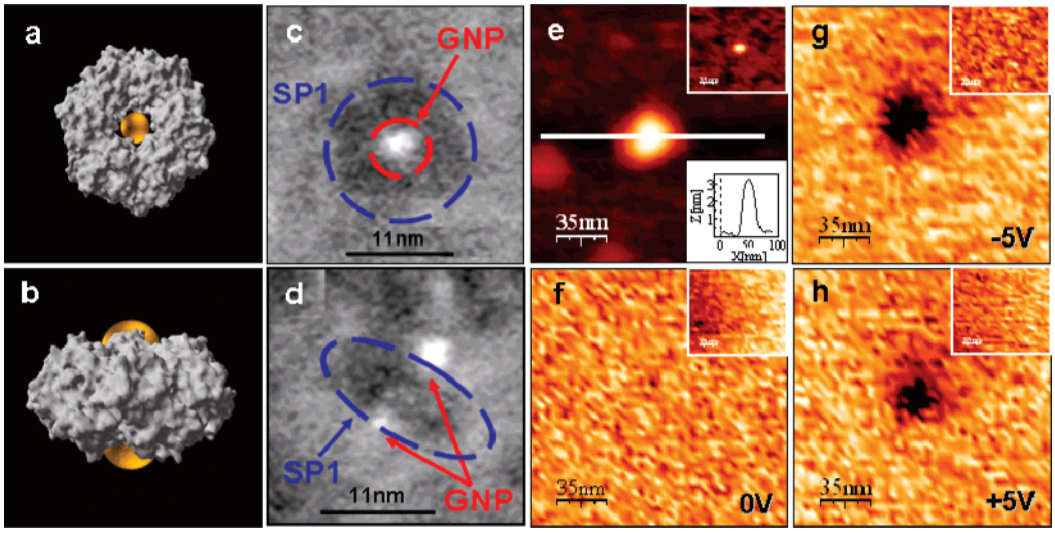

Figure 3. The 6His-SP1 gold nanoparticles hybrids. (a,b) Computer simulations of the SP1−GNP hybrid top and side views, respectively. (c,d) HAADF-STEM (vanadium staining) images of the 6His-SP1−GNP hybrid top and side views, respectively. (e) Top view AFM image of a single 6His-SP1−GNP hybrid, its cross section (lower inset) and a 6His-SP1 with no GNP attached to it (upper inset). (f−h) EFM measurements of a 6His-SP1−GNP hybrid. The phase shift images were measured 50 nm above the set point height at zero voltage (f), upon negative (−5 V) (g), and positive (+5 V) (h) voltage application. The insets show similar measurements on 6His-SP1 with no GNP attached to it, where no phase shift and therefore no electrostatic interaction signal is observed.

the *E. coli* proteins. The 6His-SP1 readily binds to Ni-NTA agarose beads and elutes out in the presence of imidazole (lane 8) in contrast to the W.T protein that displays no binding to the Ni-NTA beads (lane 6) and therefore is absent in the imidazole eluant.

The boiling stability of the 6His-SP1 is further demonstrated in Figure 2b, where we show a differential scanning calorimetry (DSC) curve of the protein at pH 7.8 in sodium phosphate buffer. DSC is a common tool for characterizing the temperature at which proteins deform and melt. This process is endothermic, and the DSC instrument compensates this loss of heat, which gives rise to a deformation peak. The observed melting temperature is very high, 109 °C, and indicates that the protein is boiling resistant. The observed melting point is close to the melting point of the recombinant W.T. SP1, 107 °C. The SDS-PAGE and DSC show that the 6His-SP1 has a similar stability profile as the W.T. SP1.[26,27,29]

The first SP1-based bioinorganic nanostructure that we formed is a hybrid of the 6His-SP1 with GNPs. Commercially available 1.8 nm GNPs covered by Ni-NTA ligands (Nanoprobes, USA) were attached to the six histidine N terminals of the 6His-SP1s. The interaction of Ni-NTA and the histidines is about $10^{-7}-10^{-13}$ M. Incubation of this variant with Ni-NTA GNPs in the presence of 3 M guanidine chloride (presumably enabling exposure of the histidine tags) targeted the GNPs to the center of the dodecamer rings. The diameter of the Ni-NTA GNP (1.8 nm) fits well into the diameter of the dodecamer inner pore (~3 nm). Such building blocks or their variants can later serve as suitable and stable building blocks for arrays such as described above or for constructing future conducting nanowires.

The 6His-SP1−GNP hybrid is visualized in Figure 3 by a variety of imaging methods. Figure 3a,b shows computer-simulated images of 6His-SP1 attached to 2 GNPs on both sides in top and side views, respectively. Figure 3 panels c and d are high-angle annular dark-field scanning transmission electron microscopy (HAADF-STEM) top and side views of 6His-SP1 GNP conjugates, respectively. The top view

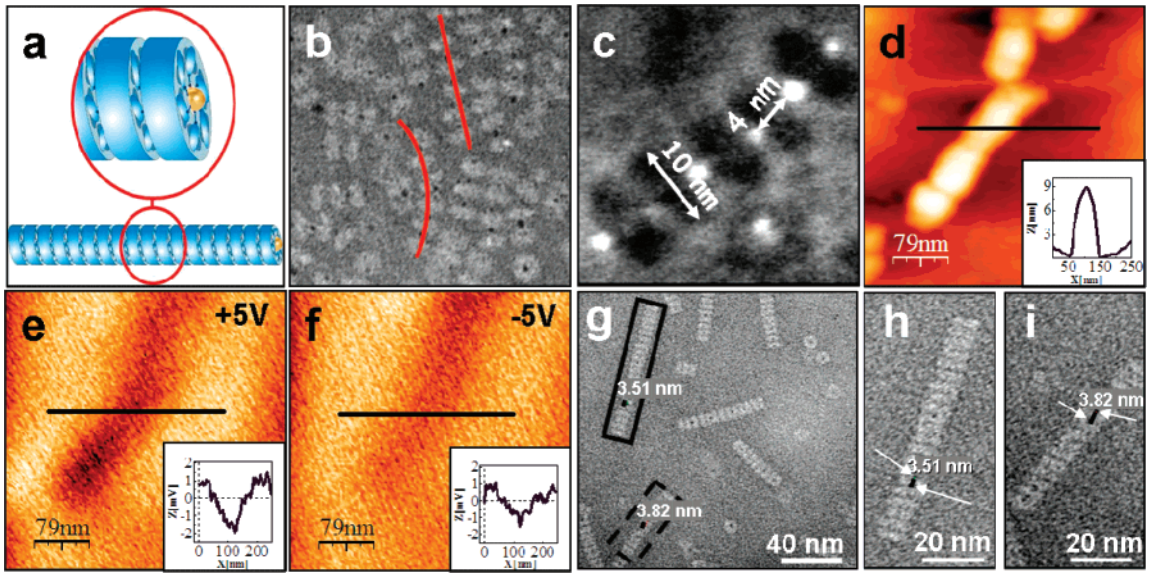

Figure 4. 6HisSP1−GNP hybrids form protein−GNP chains with different GNP separations. (a) A scheme representing the organization of protein−GNP chains composed of 6His-SP1−GNP hybrids. (b) TEM image (phosphotungstic acid staining) of 6His-SP1−GNP chains (marked by red lines). (c) HAADF-STEM image of 6His-SP1−GNP chains with 4 nm GNP separation (vanadium staining). (d) AFM image of 6His-SP1−GNP chain formation on mica (insets shows a cross-section on the chain. (e,f) EFM at positive and negative bias of 6His-SP1−GNP chain on mica, showing clear polarization of the embedded GNPs (no signal is observed at 0 V (not shown here)). The insets show the signal strength. (g) TEM image (Nanovan staining) of 6HΔSP1−GNP chains with 3.5 and 3.8 nm GNP separation. (h,i) Enlargement of the bold line boxed chains from panel g, (the arrows in panels h and i point on adjacent GNPs).

image shows the GNP (bright white) centered within the darker round protein ring. The side view (Figure 3d) shows GNPs attached to both sides of the dodecameric ring, which is consistent with the crystal structure, as there are six N-termini on each face of the 6His-SP1, pointing at opposite directions.

Dynamic mode AFM topographic characterization was performed on 6His-SP1 and on GNP-bound 6His-SP1 deposited on freshly cleaved mica surfaces. Topographic images as those in Figures 1b (measured for the W.T. SP1 but from our studies the dimensions of the W.T. SP1 and 6His-SP1 appear similar in the AFM images within our experimental resolution) and 3e show an average height (performed on several dozens of objects) of 2.3 ± 0.2 and 3.3 ± 0.2 nm for the 6His-SP1 and for the GNP-bound 6His-SP1, respectively. This is demonstrated by the cross-sections in the insets, indicating the clear difference between the two structures. The reduced height with respect to the X-ray height,[3] 4−5 nm, is probably due to surface-protein and tip-protein interactions.

An efficient noncontact and noninvasive way to identify polarizable objects, usually metal or conducting materials with AFM, is electrostatic force microscopy (EFM).[32,33] The EFM method can be used to verify the existence of the GNP in the 6His-SP1 pore. In this method, the phase shift between the induced and actual tip oscillations is recorded thus providing a sensitive indication for the tip and sample electrostatic interaction. When performing an EFM measurement, a voltage is applied to a metallized tip after raising it above the Van der Waals interaction height (∼10 nm) while the feedback is disabled. Attractive forces between the conductive tip and the probed object in both positive and negative bias voltages indicate a polarization response of the charge carriers in the measured object to the electric field. EFM measurements performed on 6His-SP1 and on GNP-bound 6His-SP1 are shown in Figure 3f−h. The EFM scan has been repeated for 0 V (Figure 3f), for −5 V (Figure 3g), and for +5 V (Figure 3h). The phase reaction above the GNP-bound 6His-SP1 location for both positive and negative bias voltages is a clear evidence for the existence of a highly polarizable object, e.g. metallic, within the 6His-SP1 protein. The lack of electrostatic signal from the 6His-SP1 (insets in Figure 3 panels f−h) ensures that the origin of the signal in the GNP-bound 6His-SP1 is from the GNP and not from the protein. The combined topographic and electrostatic information confirms the attachment of the GNP to the 6His-SP1 protein.

Once attached to the 6His-SP1, the GNP can further serve as a linker to create protein−GNP chains. Such structures are spontaneously formed upon incubation of 6His-SP1−GNP hybrids in buffer solution. The inter GNP separations within the protein−GNP chains are irregular, depending on the relative position of the GNP with regard to the protein due to the flexible long Ni-NTA linker. Figure 4a shows a scheme of a 6His-SP1−GNP protein−GNP chain. TEM image of several 6His-SP1−GNP chains can be seen in Figure 4b; the GNPs appear as dark spots between the 6His-SP1 rings (that are now "standing" in side view). HAADF-STEM image of one of the protein−GNP chains is shown in Figure 4c, where the GNPs appear as bright spots. The 6His-SP1 to 6His-SP1 (and GNP−GNP) distances are ∼4 nm.

AFM imaging of the 6His-SP1−GNP chains deposited on freshly cleaved mica surface covered with a ∼5 nm thick layer of evaporated amorphous carbon are shown in Figure 4d and reveal the expected height of the chain structure,

9−10 nm (the side profile of the "standing" 6His-SP1 ring is more resistant to the surface and tip forces so a height that is nearly the nominal diameter is measured in this case). The existence of the GNP in the 6His-SP1−GNP chain was confirmed by EFM performed in both positive and negative bias voltages, as described above and shown in Figure 4 panels e and f, respectively (no signal is observed at 0 V (not shown here)).

To improve the packing of the 6His-SP1s and to reduce the inter GNP separation (and 6His-SP1 separations), another SP1 derivative was engineered by adding a six histidine tag to a truncated N terminal SP1 (five N terminal amino acid residues were deleted from the protein, which is termed ΔNSP1) thereby forming the variant 6HΔSP1. This second variant of the SP1 protein (6His-SP1 being the first variant) should have an inner pore that may enable a deeper protrusion of the GNP into the protein pore, as 30 amino acids were deleted on each side of the SP1 ring. As expected, the protein−GNP chains composed of 6HΔSP1−GNP show shorter GNP separations in comparison with the 6His-SP1−GNP chains, as demonstrated in Figure 4g-i. The GNPs are not in contact as we still use 1.8 nm GNPs.

In this letter, we report and characterize various structures constructed from the W.T. SP1 and from two new derivatives of the SP1 protein that are utilized as a scaffold for various nanostructures: (i) A large 2D-ordered array with an 11 nm periodicity that can be useful for ultradense docking sites, for example, for nanoparticles, enzymes, or other sensors, (ii) 6His-SP1−GNP hybrids that can further serve as building blocks for various nanostructures, and (iii) Protein−GNP chains that are formed by the 6His-SP1−GNP and 6HΔSP1−GNP building blocks. Such tube-like structures with further control over the separation between the GNPs and with other GNPs diameter are promising for future investigation of electrical transport mechanisms in one-dimensional nanowires and as potential nanowires for nanoelectronics.

Acknowledgment. We thank Dr. Igor Brodsky for helpful discussions and for technical assistance. We acknowledge financial support from DFG Grant "Single Molecule based Ultra High Density Memory" CU 44/3-2 and the French Ministry of External Affairs, the Israeli-Palestinian Science Organization, and Friends of IPSO, USA (with funds donated by the Meyer Foundation).

References

(1) Bachtold, A.; Hadley, P.; Nakanishi, T.; Dekker, C. *Science* **2001**, *294* (5545), 1317−1320.
(2) Huang, Y.; Duan, X. F.; Wei, Q. Q.; Lieber, C. M. *Science* **2001**, *291* (5504), 630−633.
(3) Lieber, C. M. *Sci. Am.* **2001**, *285* (3), 58−64.
(4) Martel, R.; Schmidt, T.; Shea, H. R.; Hertel, T.; Avouris, P. *Appl. Phys. Lett.* **1998**, *73* (17), 2447−2449.
(5) McMillan, R. A.; Paavola, C. D.; Howard, J.; Chan, S. L.; Zaluzec, N. J.; Trent, J. D. *Nat. Mater.* **2002**, *1* (4), 247−252.
(6) Tucker, J. R. *J. Appl. Phys.* **1992**, *72* (9), 4399−4413.
(7) Welser, J. J.; Tiwari, S.; Rishton, S.; Lee, K. Y.; Lee, Y. *IEEE Electron Device Lett.* **1997**, *18* (6), 278−280.
(8) Persike, N.; Pfeiffer, M.; Guckenberger, R.; Radmacher, M.; Fritz, M. *J. Mol. Biol.* **2001**, *310* (4), 773−780.
(9) Thess, A.; Hutschenreiter, S.; Hofmann, M.; Tampe, R.; Baumeister, W.; Guckenberger, R. *J. Biol. Chem.* **2002**, *277* (39), 36321−36328.
(10) Yan, H. *J. Biomol. Struct. Dyn.* **2007**, *24* (6), 702−702.
(11) Lin, C. X.; Liu, Y.; Rinker, S.; Yan, H. *ChemPhysChem* **2006**, *7* (8), 1641−1647.
(12) Zhang, J. P.; Liu, Y.; Ke, Y. G.; Yan, H. *Nano Lett.* **2006**, *6* (2), 248−251.
(13) Sharma, J.; Chhabra, R.; Liu, Y.; Ke, Y. G.; Yan, H. *Angew. Chem., Int. Ed.* **2006**, *45* (5), 730−735.
(14) Seeman, N. C. *Biochemistry* **2003**, *42* (24), 7259−7269.
(15) Seeman, N. C. *Nature* **2003**, *421* (6921), 427−431.
(16) Xiao, S. J.; Liu, F. R.; Rosen, A. E.; Hainfeld, J. F.; Seeman, N. C.; Musier-Forsyth, K.; Kiehl, R. A. *J. Nanopart. Res.* **2002**, *4* (4), 313−317.
(17) Katz, E.; Willner, I. *Angew. Chem., Int. Ed.* **2004**, *43* (45), 6042−6108.
(18) Patolsky, F.; Weizmann, Y.; Lioubashevski, O.; Willner, I. *Angew. Chem., Int. Ed.* **2002**, *41* (13), 2323−2327.
(19) Braun, E.; Eichen, Y.; Sivan, U.; Ben-Yoseph, G. *Nature* **1998**, *391* (6669), 775−778.
(20) Richter, J.; Mertig, M.; Pompe, W.; Monch, I.; Schackert, H. K. *Appl. Phys. Lett.* **2001**, *78* (4), 536−538.
(21) Patolsky, F.; Weizmann, Y.; Willner, I. *Nat. Mater.* **2004**, *3* (10), 692−695.
(22) Heyman, A.; Levy, I.; Altman, A.; Shoseyov, O. *Nano Lett.* **2007**, *7* (6), 1575−1579.
(23) Lin, C. X.; Liu, Y.; Yan, H. *Nano Lett.* **2007**, *7* (2), 507−512.
(24) Jiang, G. F.; Chen, R. S.; Yan, H.; Qi, Q. Y. *Sci. China, Ser. C.: Life Sci.* **2001**, *44*, (1), 33−39.
(25) Lin, C. X.; Katilius, E.; Liu, Y.; Zhang, J. P.; Yan, H. *Angew. Chem., Int. Ed.* **2006**, *45* (32), 5296−5301.
(26) Wang, W. X.; Dgany, O.; Wolf, S. G.; Levy, I.; Algom, R.; Pouny, Y.; Wolf, A.; Marton, I.; Altman, A.; Shoseyov, O. *Biotechnol. Bioeng.* **2006**, *95* (1), 161−168.
(27) Wang, W. X.; Dgany, O.; Dym, O.; Altman, A.; Shoseyov, O.; Almog, O. *Acta Crystallogr., Sect. D* **2003**, *59* 512−514.
(28) Wang, W. X.; Pelah, D.; Alergand, T.; Shoseyov, O.; Altman, A. *Plant Physiol.* **2002**, *130* (2), 865−875.
(29) Dgany, O.; Gonzalez, A.; Sofer, O.; Wang, W. X.; Zolotnitsky, G.; Wolf, A.; Shoham, Y.; Altman, A.; Wolf, S. G.; Shoseyov, O.; Almog, O. *J. Biol. Chem.* **2004**, *279* (49), 51516−51523.
(30) Horcas, I.; Fernandez, R.; Gomez-Rodriguez, J. M.; Colchero, J.; Gomez-Herrero, J.; Baro, A. M. *Rev. Sci. Instrum.* **2007**, *78*, 013705.
(31) Brisson, A.; Olofsson, A.; Ringler, P.; Schmutz, M.; Stoylova, S. *Biol. Cell* **1994**, *80* (2−3), 221−228.
(32) Cohen, H.; Sapir, T.; Borovok, N.; Molotsky, T.; Di, Felice, R.; Kotlyar, A. B.; Porath, D. *Nano Lett.* **2007**, *7* (4), 981−986.
(33) Gomez-Navarro, C.; Moreno-Herrero, F.; de Pablo, P. J.; Colchero, J.; Gomez-Herrero, J.; Baro, A. M. *Proc. Natl. Acad. Sci. U.S.A.* **2002**, *99* (13), 8484−8487.

NL072455T